Geophysical Research Letters

RESEARCH LETTER
10.1029/2022GL102521

On the Temperature Dependence of the Cloud Ice Particle Effective Radius—A Satellite Perspective

Martin Stengel[1], Jan Fokke Meirink[2], and Salomon Eliasson[3]

[1]Deutscher Wetterdienst (DWD), Offenbach, Germany, [2]Royal Netherlands Meteorological Institute (KNMI), De Bilt, The Netherlands, [3]Swedish Meteorological and Hydrological Institute (SMHI), Norrköping, Sweden

Key Points:

- Comparisons of modeled cloud ice particle effective radius with satellite observations are presented
- For very low cloud temperatures the modeled cloud ice particle effective radius agrees on average with satellite observations
- Modeled large cloud ice particle effective radii for high sub-zero temperatures are not found in satellite observations

Correspondence to:
M. Stengel,
martin.stengel@dwd.de

Citation:
Stengel, M., Meirink, J. F., & Eliasson, S. (2023). On the temperature dependence of the cloud ice particle effective radius—A satellite perspective. *Geophysical Research Letters*, *50*, e2022GL102521. https://doi.org/10.1029/2022GL102521

Received 16 DEC 2022
Accepted 11 MAR 2023

Abstract Cloud ice particle effective radius in atmospheric models is usually parametrized. A widely-used parametrization comprises a strong dependence on the temperature. Utilizing available satellite-based estimates of both cloud ice particle effective radius and cloud-top temperature we evaluate if a similar temperature-dependence exists in these observations. We find that for very low cloud-top temperatures the modeled cloud ice particle effective radius generally agrees on average with satellite observations. For high sub-zero temperatures however, the modeled cloud ice particle effective radius becomes very large, which is not seen in the satellite observations. We conclude that the investigated parametrization for the cloud ice particle effective radius, and parametrizations with a similar temperature dependence, likely produce systematic biases at the cloud top. Supporting previous studies, our findings suggest that the vertical structure of clouds should be taken into account as factor in potential future updates of the parametrizations for cloud ice particle effective radius.

Plain Language Summary Atmospheric models are often used to diagnose and predict the atmospheric state including clouds. One very important property of clouds that consist of ice particles is the cloud ice particle effective radius. This ice effective radius is based on assumptions about the size and shapes of the ice particles in clouds, and thus parametrized, and is one of the important variables needed for calculating the effect of clouds on electromagnetic radiation, in particular on the solar radiation that enters the Earth's atmosphere. In our study we found that the parametrized ice effective radius agrees well on average and global scale with the ice effective radius inferred from satellite observations for cold clouds. However, we also found that for warmer ice clouds the parametrized ice effective radius is much higher than in satellite observations. Our study suggests that parametrizations of the ice effective radius used in atmospheric models show potential for improvements.

1. Introduction

For radiative effects of clouds, the cross-section area of the cloud particles is a critical component (Liou, 1992). Usually, scattering properties of clouds are expressed in terms of a particle effective radius (r_e), representing the mean size of a particle population. For spherical cloud particles, for example, liquid cloud droplets, r_e^{liq} is expressed by the cross-section area weighted mean radius of the cloud particles (Hansen & Travis, 1974). Ice crystals are much more complex as they appear in various shapes and habits (Bailey & Hallett, 2009). Numerous studies exist defining r_e for ice clouds $\left(r_e^{ice}\right)$, which are often related to specific assumptions about crystal habit and distributions and linked to specific radiation schemes (McFarquhar & Heymsfield, 1998). A commonly used definition for r_e^{ice} is:

$$r_e^{ice} = \frac{3}{4}\frac{IWC}{\rho_{ice} A_c} \tag{1}$$

which was proposed by Francis et al. (1994). A_c is the projected area per unit volume of the ice particle distribution.

In large scale atmospheric models, that is, those that apply single moment schemes for cloud microphysics, the explicit calculation of r_e^{ice} is usually replaced by parametrizations that relate r_e^{ice} to model bulk properties. A prominent parameterization based on in-situ measurements from aircraft campaigns is Sun and Rikus (1999), revised in Sun (2001), where r_e^{ice} depends on ice water content (IWC) and temperature (T). This parametrization is based on in-situ measurements taken by aircraft campaigns. The Sun and Rikus (1999) parametrization is widely used in global atmospheric modeling such as in the EC-Earth global climate model (Hazeleger et al., 2010), in the

ARPEGE-Climat model (Roehrig et al., 2020), in ECMWF models (Hogan & Bozzo, 2018), the FGOALS-s2 model (Bao et al., 2013) as well as in non-global models as for example, documented in Lac et al. (2018) and Bengtsson et al. (2017).

In addition to the original definition, Field et al. (2007) additionally proposed a latitude-dependent lower limit of r_e^{ice}, reflecting observations that tropical clouds might typically have larger ice/snow particles than clouds in the Extratropics. Independent of the latter, a pronounced T-dependence continues to be imposed on r_e^{ice} in this parametrization.

van Zadelhoff et al. (2004) investigated ground-based observations of r_e^{ice} at Cloudnet and ARM sites for ice clouds with optical depth smaller than 4. They found r_e^{ice} to be dependent on the vertical position within the cloud layer, with largest values in the middle of the cloud. They also found a pronounced T-dependence of r_e^{ice} (positively correlated) in the middle sections of the clouds. However, that dependence nearly vanishes at cloud bottom and cloud top, suggesting that the relation of r_e^{ice} to T has a vertical structure within clouds and, by extension, suggesting that a single r_e^{ice} parametrization might be inappropriate for some parts of the clouds; for example, a parametrization that features a strong dependence of r_e^{ice} from T might be inappropriate at cloud top and cloud bottom. As the cloud processes are likely to be different in different parts of the clouds, the results of van Zadelhoff et al. (2004) seem not surprising.

In this study, we extend the observation-driven analysis of the T-dependence of r_e^{ice} to all ice clouds and to global scales using satellite observations of both r_e^{ice} and cloud top temperature (CTT). These two cloud top properties are retrieved independently in the three satellite-based cloud datasets used in our study. Acknowledging that the satellite-based cloud data used in this study are retrieval estimates associated with retrieval uncertainties, we will use the term satellite observations throughout the manuscript for convenience.

2. Data and Methods

2.1. Modeled r_e^{ice}

In large-scale atmospheric models, r_e^{ice} is widely parametrized as a function of T and IWC as formulated by Sun and Rikus (1999) and Sun (2001):

$$r_e^{ice} = f(T, IWC, p) \tag{2}$$

When the IWC is given in kg/kg, the conversion to g/m^3 introduces an additional, although relatively weak, sensitivity of r_e^{ice} to the air pressure (p) via the air density needed in that conversion. Appendix A elaborates Equation 2, which reveals that the dependence of r_e^{ice} on T is fairly strong, with increasing T leading to increasing r_e^{ice}. This is visualized in Figure 1, showing r_e^{ice} as a function of T and IWC calculated using Equation 2 for arbitrary, although realistic, values of T and IWC. The results are first shown for IWC given in g/m^3 (panel a), and second for IWC given in g/kg at three pressure levels representing high-, mid-, and low-level clouds (panels b–d).

2.2. Satellite-Observed r_e^{ice}

This study used three satellite datasets, with the restriction that these products contain both r_e^{ice} and CTT with global coverage. This is generally only feasible with satellite-borne, passive imaging sensors that measure in the visible through to the infrared spectral range, such as the Moderate Resolution Imaging Spectroradiometer (MODIS) and the Advanced Very High Resolution Radiometer (AVHRR), onboard polar-orbiting satellites. Furthermore, our study required for each potential data set individually that both properties (r_e^{ice} and CTT) are independently retrieved. The eventually selected datasets are listed in Table 1 and comprise of Cloud_cci AVHRR-PMv3 (Stengel et al., 2020), CLARA-A2 (Karlsson et al., 2017b) and MODIS Collection 6.1 (C6.1) (Baum et al., 2012; Marchant et al., 2016; Platnick, Meyer, et al., 2017). Cloud_cci and CLARA-A2 provide global composites of the cloud properties of interest on a 0.05° × 0.05° grid as part of their product portfolio from which only NOAA-19 data was used. MODIS Aqua C6.1 swath data (Level-2) products were pre-processed for this study before usage to represent the same global composite. The used data includes all the days of July 2011, with the results being nearly identical when using less or more data and other seasons or years. As solar illumination is required to retrieve r_e^{ice}, night-time data is not included in our study.

It is important to note that while for all three datasets r_e^{ice} is defined as given in Equation 1, all three datasets are based on different assumptions regarding the ice crystal habit. Cloud_cci uses the General Habit Mixture (Baum

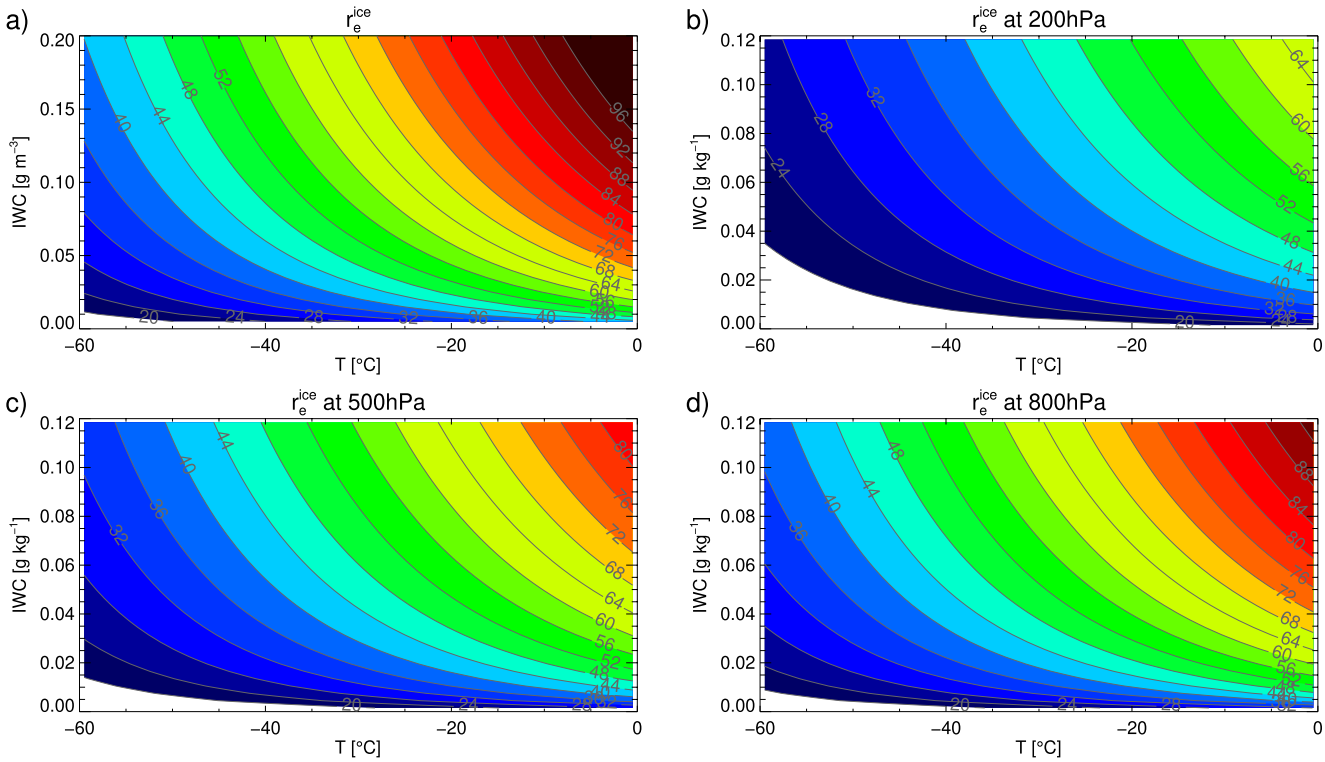

Figure 1. (a) Modeled ice effective radius $\left(r_e^{ice}\right)$ in μm as function of temperature and cloud water content (given in g m^{-3}) following Sun and Rikus (1999). (b) to (d) Modeled ice effective radius (in μm) as function of temperature and cloud water content when given in g kg^{-1} at 200 hPa (b), 500 hPa (c) and 800 hPa (d). In atmospheric models the cloud water content is often given in g kg^{-1}, thus a small air pressure dependency is introduced into the calculation of the effective radius as the conversion from g kg^{-1} to g m^{-3} requires the air density which is a function of pressure.

et al., 2011, 2014), aggregated over a collection of observed particle size distributions. MODIS C6.1 uses aggregates of solid hexagonal columns (Yang et al., 2013), also with a collection of observed particle size distributions. CLARA-A2 uses monodisperse distributions of hexagonal columns (Hess et al., 1998). Similar to CLARA-A2, Sun and Rikus (1999) also assume hexagonal columns with a size distributions following McFarquhar and Heymsfield (1997).

Table 1
Observational Satellite Data Sets Used in This Study, Each Containing Cloud Ice Particle Effective Radius r_e^{ice} (at 3.7 μm) and Cloud Top Temperature (CTT)

Data set/Product	Reference	Comment
Cloud_cci AVHRR-PMv3 Level-3U (NOAA-19 subset)	Stengel et al. (2020)	Level-3U is a global composite product, from which r_e^{ice}, CTT and CTP of each cloudy pixel were collected when of ice phase and uncertainties for cloud detection and phase not exceeding 30%
CM SAF CLARA-A2 Level-2b (NOAA-19 subset)	Karlsson et al. (2017b)	CLARA Level-2b product is also a global composite product. Also here, r_e^{ice}, CTT and CTP of each cloudy pixel were collected when of ice phase. No further quality indicators were available/utilized.
MODIS Collection 6.1 Level-2 (Aqua satellite)	Baum et al. (2012), Marchant et al. (2016), Platnick, Meyer, et al. (2017)	The pixel-based MODIS retrievals of the MYD06 swath product have been collected in time windows of 24 hours to compose daily global composites, basically mimicking the Level-3U/Level-2b products of the datasets above.

Note. Additionally, cloud top pressure (CTP) was extracted to do the stratification by low-, mid- and high-level cloud layers. All data were from July 2011.

Since all three observational datasets are based on passive VIS-IR imaging satellite sensors, they represent the cloud properties near the cloud top only. As this limitation cannot be circumvented, model fields, to which we will compare the satellite observations, have been processed with a satellite simulator to facilitate a fair comparison with more corresponding information given in Section 2.3.

It needs to be mentioned that some uncertainty in quantifying random and systematic errors in the satellite retrievals of ice particle effective radius exists, as there is no ultimate reference data source available. Very few inter-comparison study exist. Kahn et al. (2015), for example, compared MODIS r_e^{ice} with infrared-based retrievals from the Atmospheric Infrared Sounder (AIRS). While the MODIS r_e^{ice} derived from the 2.1 micron band was found to be 5–10 μm larger than the AIRS r_e^{ice}, the MODIS 3.7-micron-derived r_e^{ice} (as used in this study) was largely unbiased.

2.3. Processing Model Fields Through a Satellite Simulator

In this study, the SIMFERA satellite simulator (Stengel et al., 2018) was applied to 6-hourly, un-averaged ERA-Interim data (Dee et al., 2011). The application of the satellite simulator is necessary to identify the cloud top level consistent with the satellite products, for example, to infer cloud-top temperature. The satellite simulator also includes the computation of r_e^{ice} using the Sun and Rikus (1999) parametrization with the reanalysis cloud fields, that is, IWC and temperature, as input.

Even though the modeled clouds in ERA-Interim might have caveats, we believe that for the comparisons conducted in the study it is not of critical importance to have all individual clouds modeled absolutely correctly, but rather represent the general distribution of cloudiness in space and time, which was shown for ERA-Interim in Stengel et al. (2018).

3. Results and Discussion

Figure 2 shows the globally collected r_e^{ice} as a function of CTT, only excluding the polar regions south of 60°S and north of 60°N. For each CTT bin, the mean r_e^{ice} is given along with the underlying distribution represented by box plots showing 5%, 25%, 50%, 75%, 95% percentiles. Analyzing the model data, the strong dependence of r_e^{ice} on CTT, as given in Equation 2 and as shown in Figure 1, is preserved in the simulator output in Figure 2, with low (high) r_e^{ice} values for low (high) temperatures. The observations of r_e^{ice} agree well with the modeled ones for low temperatures (below −40°C) in terms of mean values per CTT bin, with MODIS C6 presenting slightly higher values than the other datasets, CLARA-A2 and Cloud_cci. The spread, however, is larger in all observational datasets than for the modeled clouds for this temperature range.

Considering the temperature range from −40° to 0°C, the deviation between observed and modeled r_e^{ice} becomes very large. The modeled r_e^{ice} describes a nearly linear function with r_e^{ice} increasing more than 1 μm per K. At high sub-zero temperatures, the modeled r_e^{ice} have a mean near 70 μm. In contrast, the observed r_e^{ice} remain nearly unchanged for warm sub-zero temperatures. The scatter among the observational datasets is small for the mean values and for the underlying distribution in each temperature bin, and the scatter is much smaller than the deviation to the modeled r_e^{ice}. The fact that the observational datasets have all different ice crystal habit assumptions, while Sun and Rikus (1999) use the same particles as CLARA-A2 (see Section 2.2), suggests that the assumed habit cannot explain the found deviations between observed and modeled r_e^{ice}. To emphasize the importance of the findings we analyzed that about 23% of all clouds in the reanalysis data used in our study have an ice cloud top and a CTT in the range from −40°C to 0°C. Thus the findings above concern almost one fourth of all clouds.

For high-level clouds, the observational datasets show a slight tendency to give lower r_e^{ice} for higher temperatures. This feature is most pronounced for Cloud_cci and for this data set visible for mid-level clouds as well. It is not completely known yet what the cause of this feature could be. It cannot be ruled out that all observational datasets are affected by the same caveat; the possible contaminations by sub-pixel liquid cloud phase in pixels associated with ice phase. Coopman et al. (2019) found that binary phase information has the potential to lead to a low bias in r_e^{ice} when liquid phase constitutes parts of the satellite pixel. However, this effect is too small to explain the large difference found between observations and modeled clouds for higher sub-zero temperatures. Furthermore, for the Cloud_cci data, which show the most pronounced drop in r_e^{ice} at higher sub-zero temperatures, we analyzed by comparison with Cloud-Aerosol Lidar with Orthogonal Polarization (Winker et al., 2009) observations that only about 9% of the clouds with CTT between −40°C and 0°C are potentially misclassified as ice.

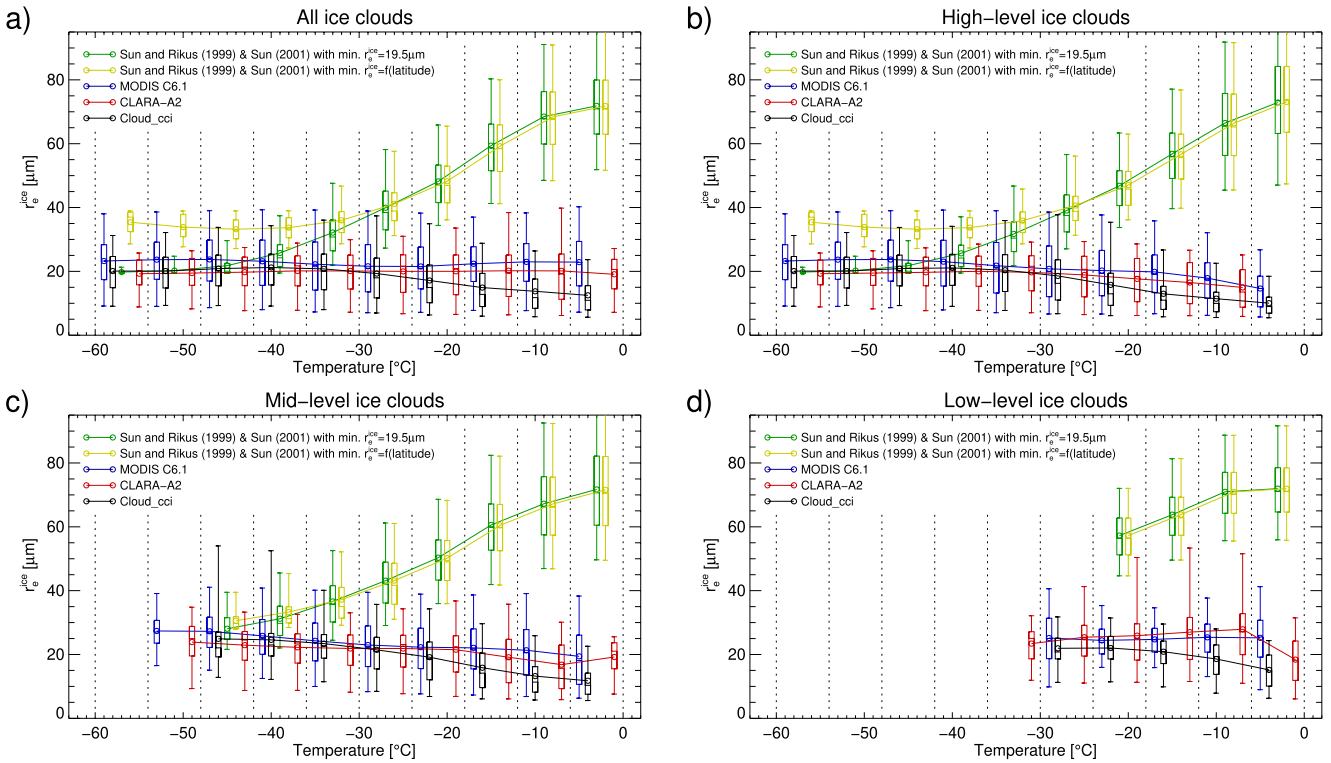

Figure 2. Modeled and observed ice effective radius $\left(r_e^{ice}\right)$ shown as mean (circles) and box-plot (5%, 25%, 50%, 75%, 95% percentiles) for given cloud-top temperature (CTT) bins with bin width of 6°C (vertical dashed lines) for all cloud levels (a) and stratified by high-level (b), mid-level (c) and low-level (d) clouds. All data is for ±60° latitude.

4. Summary and Conclusions

In this study, we have used global satellite datasets of CTT and cloud top r_e^{ice} to evaluate the strong temperature dependence in a commonly used parametrization of r_e^{ice}. Modeled clouds from ERA-Interim were processed through a satellite simulator to represent (near-) cloud-top information as in the observations and to apply the parametrization. While for cloud temperature below −40°C, the modeled r_e^{ice} roughly agrees to the observations, the strong temperature dependence that governs the modeled r_e^{ice} makes them very large for warmer sub-zero temperatures. We do not see any indication in the observations that this is generally the case. The observations suggest nearly a constant cloud top r_e^{ice} throughout the sub-zero temperature range. Our results extend the findings of an earlier study, that was limited to measurements at a few ground sites, to global scales. Though we do not want to rule out, that for some cloud types such a temperature dependence of the cloud top r_e^{ice} exists, it is certainly not generally the case on a global scale. Furthermore, as we only investigated the cloud top layers, r_e^{ice} might be temperature-dependent further down into the clouds. However, our results clearly indicate that cloud top r_e^{ice} might not be as temperature-dependent as currently implied by a commonly applied parametrization. Thus we suggest revising this parametrization and similar ones to include information on the vertical structure of the clouds and thus potentially to reflect the small temperature dependence of r_e^{ice} near the cloud top as found in the presented study. As van Zadelhoff et al. (2007) have shown, modifications in the parametrization of the cloud ice particle effective radius can have a modest but significant positive impact on the simulated shortwave radiation budget. However, it might not always be easy to demonstrate the improvements.

Appendix A: r_e^{ice} Parametrization

The parametrization for r_e^{ice} formulated by Sun and Rikus (1999) and revised by Sun (2001):

$$
\begin{aligned}
ZIWC &= IWC * RHOAIR * 1000. \\
ZRefDe &= 0.64952 \\
ZTEMPC &= PT - 83.15 \\
ZTCELS &= PT - RTT \\
ZFSR &= 1.2351 + 0.0105 * ZTCELS \\
ZAIWC &= 45.8966 * \left(ZIWC^{0.2214}\right) \\
ZBIWC &= 0.7957 * \left(ZIWC^{0.2535}\right) \\
ZDESR &= ZFSR * (ZAIWC + ZBIWC * ZTEMPC) \\
ZDESR &= (30. > ZDESR < 155.) \\
r_e^{ice} &= ZRefDe * ZDESR
\end{aligned}
\tag{A1}
$$

With r_e^{ice} being dependent on ice water content (IWC) in kg/kg, the air density (RHOAIR) in kg/m^3, the air temperature (PT) in K and RTT which is 273 K. The boundaries applied to ZDESR imply that r_e^{ice} is between 19.5 and 100.7 µm. Slight deviations of Equation A1 might be implemented in different models.

Data Availability Statement

The satellite simulator SIMFERA code is available through GitHub: https://github.com/martinstengel/simfera/releases/tag/v1.0. A permanent deposition of this code is available through this DOI: https://doi.org/10.5281/zenodo.7445152. The satellite data used in this study are freely and openly available: Cloud_cci AVHRR-PMv3 Level-3U: https://doi.org/10.5676/DWD/ESA_Cloud_cci/AVHRR-PM/V003 (Stengel et al., 2019) CM SAF CLARA-A2 Level-2b: https://doi.org/10.5676/EUM_SAF_CM/CLARA_AVHRR/V002 (Karlsson et al., 2017a) MODIS Collection 6.1 Level-2: http://doi.org/10.5067/MODIS/MYD06_L2.NRT.061 (Platnick, King, et al., 2017).

Acknowledgments
The authors acknowledge the availability of the Cloud_cci AVHRR-PMv3 data through the ESA Climate Change Initiative programme, the CLARA-A2 data through the EUMETSAT Satellite Application Facility on Climate Monitoring (CM SAF) and the MODIS Collection 6.1 data through the National Aeronautics and Space Administration (NASA). The contribution of MS to this study was supported by the European Space Agency (ESA) through the Cloud_cci project (contract no.: 4000128637/20/I-NB). Open Access funding enabled and organized by Projekt DEAL.

References

Bailey, M. P., & Hallett, J. (2009). A comprehensive habit diagram for atmospheric ice crystals: Confirmation from the laboratory, AIRS II, and other field studies. *Journal of the Atmospheric Sciences*, *66*(9), 2888–2899. https://doi.org/10.1175/2009JAS2883.1

Bao, Q., Lin, P., Zhou, T., Liu, Y., Yu, Y., Wu, G., et al. (2013). The flexible global ocean-atmosphere-land system model, spectral version 2: Fgoals-s2. *Advances in Atmospheric Sciences*, *30*(3), 561–576. https://doi.org/10.1007/s00376-012-2113-9

Baum, B. A., Menzel, W. P., Frey, R. A., Tobin, D. C., Holz, R. E., Ackerman, S. A., et al. (2012). MODIS cloud-top property refinements for collection 6. *Journal of Applied Meteorology and Climatology*, *51*(6), 1145–1163. https://doi.org/10.1175/JAMC-D-11-0203.1

Baum, B. A., Yang, P., Heymsfield, A. J., Bansemer, A., Cole, B. H., Merrelli, A., et al. (2014). Ice cloud single-scattering property models with the full phase matrix at wavelengths from 0.2 to 100 µm. *Journal of Quantitative Spectroscopy and Radiative Transfer*, *146*, 123–139. https://doi.org/10.1016/j.jqsrt.2014.02.029

Baum, B. A., Yang, P., Heymsfield, A. J., Schmitt, C. G., Xie, Y., Bansemer, A., et al. (2011). Improvements in shortwave bulk scattering and absorption models for the remote sensing of ice clouds. *Journal of Applied Meteorology and Climatology*, *50*(5), 1037–1056. https://doi.org/10.1175/2010jamc2608.1

Bengtsson, L., Andrae, U., Aspelien, T., Batrak, Y., Calvo, J., de Rooy, W., et al. (2017). The HARMONIE–AROME model configuration in the ALADIN–HIRLAM NWP system. *Monthly Weather Review*, *145*(5), 1919–1935. https://doi.org/10.1175/mwr-d-16-0417.1

Coopman, Q., Hoose, C., & Stengel, M. (2019). Detection of mixed-phase convective clouds by a binary phase information from the passive geostationary instrument SEVIRI. *Journal of Geophysical Research: Atmospheres*, *124*(9), 5045–5057. https://doi.org/10.1029/2018jd029772

Dee, D. P., Uppala, S. M., Simmons, A. J., Berrisford, P., Poli, P., Kobayashi, S., et al. (2011). The ERA-interim reanalysis: Configuration and performance of the data assimilation system (Vol. *137*, pp. 553–597). https://doi.org/10.1002/qj.828

Field, P. R., Heymsfield, A. J., & Bansemer, A. (2007). Snow size distribution parameterization for midlatitude and tropical ice clouds. *Journal of the Atmospheric Sciences*, *64*(12), 4346–4365. https://doi.org/10.1175/2007JAS2344.1

Francis, P., Jones, A., Saunders, R., Shine, K., Slingo, A., & Sun, Z. (1994). An observational and theoretical study of the radiative properties of cirrus: Some results from ICE'89. *Quarterly Journal of the Royal Meteorological Society*, *120*(518), 809–848. https://doi.org/10.1002/qj.49712051804

Hansen, J. E., & Travis, L. D. (1974). Light scattering in planetary atmospheres. *Space Science Reviews*, *16*(4), 527–610. https://doi.org/10.1007/bf00168069

Hazeleger, W., Severijns, C., Semmler, T., Ştefănescu, S., Yang, S., Wang, X., et al. (2010). EC-Earth. *Bulletin of the American Meteorological Society*, *91*(10), 1357–1364. https://doi.org/10.1175/2010BAMS2877.1

Hess, M., Koelemeijer, R. B., & Stammes, P. (1998). Scattering matrices of imperfect hexagonal ice crystals. *Journal of Quantitative Spectroscopy and Radiative Transfer*, *60*(3), 301–308. https://doi.org/10.1016/s0022-4073(98)00007-7

Hogan, R. J., & Bozzo, A. (2018). A flexible and efficient radiation scheme for the ECMWF model. *Journal of Advances in Modeling Earth Systems*, *10*(8), 1990–2008. https://doi.org/10.1029/2018MS001364

Kahn, B., Schreier, M., Yue, Q., Fetzer, E., Irion, F., Platnick, S., et al. (2015). Pixel-scale assessment and uncertainty analysis of airs and MODIS ice cloud optical thickness and effective radius. *Journal of Geophysical Research: Atmospheres*, *120*(22), 11–669. https://doi.org/10.1002/2015jd023950

Karlsson, K.-G., Anttila, K., Trentmann, J., Stengel, M., Meirink, J. F., Devasthale, A., et al. (2017a). CLARA-A2: CM SAF cLoud, Albedo and surface RAdiation dataset from AVHRR data—Edition 2, satellite application facility on climate monitoring. https://doi.org/10.5676/EUM_SAF_CM/CLARA_AVHRR/V002

Karlsson, K.-G., Anttila, K., Trentmann, J., Stengel, M., Meirink, J. F., Devasthale, A., et al. (2017b). CLARA-A2: The second edition of the CM SAF cloud and radiation data record from 34 years of global AVHRR data. *Atmospheric Chemistry and Physics*, *17*(9), 5809–5828. https://doi.org/10.5194/acp-17-5809-2017

Lac, C., Chaboureau, J.-P., Masson, V., Pinty, J.-P., Tulet, P., Escobar, J., et al. (2018). Overview of the Meso-NH model version 5.4 and its applications. *Geoscientific Model Development*, *11*(5), 1929–1969. https://doi.org/10.5194/gmd-11-1929-2018

Liou, K.-N. (1992). *Radiation and cloud processes in the atmosphere. Theory, observation, and modeling* (p. 504). Oxford University Press.

Marchant, B., Platnick, S., Meyer, K., Arnold, G. T., & Riedi, J. (2016). MODIS collection 6 shortwave-derived cloud phase classification algorithm and comparisons with CALIOP. *Atmospheric Measurement Techniques*, *9*(4), 1587–1599. https://doi.org/10.5194/amt-9-1587-2016

McFarquhar, G. M., & Heymsfield, A. J. (1997). Parameterization of tropical cirrus ice crystal size distributions and implications for radiative transfer: Results from CEPEX. *Journal of the Atmospheric Sciences*, *54*(17), 2187–2200. https://doi.org/10.1175/1520-0469(1997)054<2187:potcic>2.0.co;2

McFarquhar, G. M., & Heymsfield, A. J. (1998). The definition and significance of an effective radius for ice clouds. *Journal of the Atmospheric Sciences*, *55*(11), 2039–2052. https://doi.org/10.1175/1520-0469(1998)055<2039:TDASOA>2.0.CO;2

Platnick, S., King, M., Wind, G., Ackerman, S., Menzel, P., & Frey, R. (2017). MODIS atmosphere L2 cloud product (06_L2). In *NASA MODIS adaptive processing system*. Goddard Space Flight Center. https://doi.org/10.5067/MODIS/MYD06_L2.NRT.061

Platnick, S., Meyer, K. G., King, M. D., Wind, G., Amarasinghe, N., Marchant, B., et al. (2017). The MODIS cloud optical and microphysical products: Collection 6 updates and examples from Terra and Aqua. *IEEE Transactions on Geoscience and Remote Sensing*, *55*(1), 502–525. https://doi.org/10.1109/TGRS.2016.2610522

Roehrig, R., Beau, I., Saint-Martin, D., Alias, A., Decharme, B., Guérémy, J.-F., et al. (2020). The CNRM global atmosphere model ARPEGE-Climat 6.3: Description and evaluation. *Journal of Advances in Modeling Earth Systems*, *12*(7), e2020MS002075. https://doi.org/10.1029/2020MS002075

Stengel, M., Schlundt, C., Stapelberg, S., Sus, O., Eliasson, S., Willén, U., & Meirink, J. F. (2018). Comparing era-interim clouds with satellite observations using a simplified satellite simulator. *Atmospheric Chemistry and Physics*, *18*(23), 17601–17614. https://doi.org/10.5194/acp-18-17601-2018

Stengel, M., Stapelberg, S., Sus, O., Finkensieper, S., Würzler, B., Philipp, D., et al. (2020). Cloud_cci advanced very high resolution radiometer post meridiem (AVHRR-PM) dataset version 3: 35-year climatology of global cloud and radiation properties. *Earth System Science Data*, *12*(1), 41–60. https://doi.org/10.5194/essd-12-41-2020

Stengel, M., Sus, O., Stapelberg, S., Finkensieper, S., Würzler, B., Philipp, D., et al. (2019). ESA cloud climate change initiative (ESA Cloud_cci) data: Cloud_cci AVHRR-PM L3C/L3U PRODUCTS v3.0, Deutscher Wetterdienst (DWD). https://doi.org/10.5676/DWD/ESA_Cloud_cci/AVHRR-PM/V003

Sun, Z. (2001). Reply to comments by Greg M. McFarquhar on "Parametrization of effective sizes of cirrus-cloud particles and its verification against observations." (October B, 1999,125, 3037 3055). *Quarterly Journal of the Royal Meteorological Society*, *127*(571), 267–271. https://doi.org/10.1002/qj.49712757116

Sun, Z., & Rikus, L. (1999). Parametrization of effective sizes of cirrus-cloud particles and its verification against observations. *Quarterly Journal of the Royal Meteorological Society*, *125*(560), 3037–3055. https://doi.org/10.1002/qj.49712556012

van Zadelhoff, G.-J., Donovan, D. P., Klein Baltink, H., & Boers, R. (2004). Comparing ice cloud microphysical properties using CloudNET and atmospheric radiation measurement program data. *Journal of Geophysical Research*, *109*(D24), D24214. https://doi.org/10.1029/2004JD004967

van Zadelhoff, G.-J., Van Meijgaard, E., Donovan, D., Knap, W., & Boers, R. (2007). Sensitivity of the shortwave radiative budget to the parameterization of ice crystal effective radius. *Journal of Geophysical Research*, *112*(D8), D08213. https://doi.org/10.1029/2006jd007791

Winker, D. M., Vaughan, M. A., Omar, A., Hu, Y., Powell, K. A., Liu, Z., et al. (2009). Overview of the CALIPSO mission and CALIOP data processing algorithms. *Journal of Atmospheric and Oceanic Technology*, *26*(11), 2310–2323. https://doi.org/10.1175/2009JTECHA1281.1

Yang, P., Bi, L., Baum, B. A., Liou, K.-N., Kattawar, G. W., Mishchenko, M. I., & Cole, B. (2013). Spectrally consistent scattering, absorption, and polarization properties of atmospheric ice crystals at wavelengths from 0.2 to 100 μ m. *Journal of the Atmospheric Sciences*, *70*(1), 330–347. https://doi.org/10.1175/jas-d-12-039.1